JOURNAL OF VIROLOGY, Mar. 2007, p. 2675–2687 Vol. 81, No. 6
0022-538X/07/$08.00+0 doi:10.1128/JVI.02245-06

Spatiotemporal Analysis of Purkinje Cell Degeneration Relative to Parasagittal Expression Domains in a Model of Neonatal Viral Infection▽

Brent L. Williams, Kavitha Yaddanapudi, Mady Hornig, and W. Ian Lipkin*

Jerome L. and Dawn Greene Infectious Disease Laboratory, Mailman School of Public Health, Columbia University, New York, New York

Received 12 October 2006/Accepted 11 December 2006

Infection of newborn Lewis rats with Borna disease virus (neonatal Borna disease [NBD]) results in cerebellar damage without the cellular inflammation associated with infections in later life. Purkinje cell (PC) damage has been reported for several models of early-life viral infection, including NBD; however, the time course and distribution of PC pathology have not been investigated rigorously. This study examined the spatiotemporal relationship between PC death and zonal organization in NBD cerebella. Real-time PCR at postnatal day 28 (PND28) revealed decreased cerebellar levels of mRNAs encoding the glycolytic enzymes aldolase C (AldoC, also known as zebrin II) and phosphofructokinase C and the excitatory amino acid transporter 4 (EAAT4). Zebrin II and EAAT4 immunofluorescence analysis in PND21, PND28, PND42, and PND84 NBD rat cerebella revealed a complex pattern of PC degeneration. Early cell loss (PND28) was characterized by preferential apoptotic loss of zebrin II/EAAT4-negative PC subsets in the anterior vermis. Consistent with early preferential loss of zebrin II/EAAT4-negative PCs in the vermis, the densities of microglia and the Bergmann glial expression of metallothionein I/II and the hyaluronan receptor CD44 were higher in zebrin II/EAAT4-negative zones. In contrast, early loss in lateral cerebellar lobules did not reflect a similar discrimination between PC phenotypes. Patterns of vermal PC loss became more heterogeneous at PND42, with the loss of both zebrin II/EAAT4-negative and zebrin II/EAAT4-positive neurons. At PND84, zebrin II/EAAT4 patterning was abolished in the anterior cerebellum, with preferential PC survival in lobule X. Our investigation reveals regional discrimination between patterns of PC subset loss, defined by zebrin II/EAAT4 expression domains, following neonatal viral infection. These findings suggest a differential vulnerability of PC subsets during the early stages of virus-induced neurodegeneration.

Borna disease virus (BDV) is a neurotropic RNA virus that causes persistent infection in a wide variety of warm-blooded animals. Manifestations of infection differ with the age at the time of infection. Whereas adult infected rats have an immunomediated, frequently fatal meningoencephalitis with profound generalized neuronal loss (Borna disease), rats infected in the first 24 h of life have a more subtle disorder (neonatal Borna disease [NBD]). BDV is not a lytic virus; nonetheless, NBD is attended by apoptotic neuronal death in the hippocampus (HC), neocortex, and cerebellum (CBLM) (17, 29, 73). Purkinje cell (PC) loss is a hallmark of NBD, with approximately 75% attrition by 7 months postinfection (17). Cerebellar pathology is also reported for mumps virus, lymphocytic choriomeningitis virus, reovirus, and parvovirus infections (10, 44, 49, 55, 65). In contrast to NBD, where PCs appear to be the primary target of BDV infection and cerebellar pathology reflects cytoarchitectural disruption and PC loss through apoptosis, PC pathology in LCMV infection is immune cell mediated, and parvovirus-associated PC damage is attributed to secondary effects of selective infection and destruction of granule cell neurons (10, 44). Until recently, specific mechanisms contributing to apoptotic PC death in NBD remained poorly defined. A recent report by our laboratory demonstrated the induction of endoplasmic reticulum (ER) stress in infected PCs associated with an imbalance between apoptotic signals and ER quality control functions (77).

The CBLM has traditionally been considered the center for coordination of somatic motor function and balance. However, connections between the CBLM and nonmotor cortical and subcortical structures, combined with cerebellar pathology and associated neuropsychiatric deficits, suggest the potential for cerebellar participation in cognitive and affective processing (36, 62). Infection-induced motor and balance deficits reported in NBD rats include locomotor hyperactivity, ataxia, abnormalities in bar-holding and bar-crossing abilities, righting, and geotaxis responses (7, 29, 48). Deficits in learning, memory, emotional responses, and social and stereotypic behaviors have also been reported (13, 29, 46, 47, 54).

Substantial cerebellar development in the rat is postnatal. PCs are formed prenatally at embryonic days 13 to 15 (E13 to E15), but the characteristic monolayer alignment is not achieved until postnatal days 4 to 8 (PND4-8). PC dendrites also develop postnatally, reaching adult dimensions after PND15; synaptogenesis with parallel fibers of granule cells, granule cell proliferation, and elimination of supernumerary climbing fibers continue well into the third postnatal week (20, 37).

Histologically, the CBLM is defined by a uniform layered

* Corresponding author. Mailing address: Jerome L. and Dawn Greene Infectious Disease Laboratory, Mailman School of Public Health, Columbia University, 722 West 168th Street, Rm. 1801, New York, NY 10032. Phone: (212) 342-9033. Fax: (212) 342-9044. E-mail: wil2001@columbia.edu.

▽ Published ahead of print on 20 December 2006.

TABLE 1. Rat gene-specific primers and probes for real-time PCR

Gene (GenBank accession no.)	Primer pair (5′–3′) (reaction concn) and probe[a]	Amplicon size (bp)
AldoC (NM_012497)	For, ACCTGGAAGGGACTCTCCTCA (900 nM) Rev, AAGTCACCCCTGGGACAGCT (900 nM) FAM-ACTGTCACTGCCCTGCGTCGAACTGT-TAMRA	140
EAAT4 (U89608)	For, CCAGCTCTGCAACTCTGCCT (300 nM) Rev, GCAATAAAGATGGCTGCCAAG (300 nM) FAM-ACATGGACGGCACCGCGCTCT-TAMRA	150
PFK-C (L25387)	For, TGCATTTGACAGGATTTTGGC (300 nM) Rev, CTGGGTCATTTGCACGCAC (300 nM) FAM-ACTGAGAGGAAATCAAGCTGTACGCCTGC-TAMRA	150
PBGD (X06827)	For, ATTCGGGGAAACCTCAACACC (300 nM) Rev, CTGACCCACAGCATACATGCAT (300 nM) FAM-GCAAGATCTGGCCCACCCGGTT-TAMRA	157

[a] For, forward primer; Rev, reverse primer.

architecture. However, a more complex cerebellar compartmentalization into parasagittal expression domains is apparent with immunocytochemical markers (i.e., zebrin II, EAAT4, HSP25, HNK-1, mGlur1b, etc.) that discriminate between subsets of PC neurons (58). Zebrin II is the most extensively studied of these markers. Cloning and expression studies have identified the zebrin II gene as encoding the glycolytic enzyme AldoC, which catalyzes the cleavage of fructose 1,6-bisphosphate into D-glyceraldehyde phosphate and dihydroacetone phosphate (1). In adult rodents, zebrin expression in PCs manifests in a pattern of 13 parasagittal bands with symmetry about the midline (35). Transverse boundaries of zebrin II expression are divided into the anterior zone (AZ; lobules I to V), central zone (CZ; lobules VI and VII), posterior zone (PZ; lobule VIII), and nodular zone (NZ; lobules IX and X). The AZ is characterized by narrow bands of zebrin II-positive PCs (designated P1 to P7) interdigitating with broad bands of zebrin II-negative PCs. The opposite is true of the PZ, where broad bands of zebrin II-positive neurons interdigitate with narrow zebrin II-negative bands. PCs in the CZ, NZ, and paraflocculi/flocculi are uniformly zebrin II positive. In animal models in which PC loss predominates, cell death may be random or organized, with preferential degeneration of PC subsets (58). However, compartmentalization of PC loss in response to viral infection of the central nervous system has not previously been investigated.

In this study, we examined patterns of PC death in NBD rats relative to parasagittal expression domains. Our analysis revealed spatiotemporally defined patterns of PC loss and apoptosis in association with zebrin II and excitatory amino acid transporter 4 (EAAT4) PC phenotypes. These findings suggest differential stage- and region-specific vulnerabilities of PC subsets and may provide insights into mechanisms of PC death in infections during early life.

MATERIALS AND METHODS

Animals and virus. Lewis rat dams were obtained from Charles River Laboratories (Wilmington, MA). Within 12 h of birth, 81 Lewis rat pups were inoculated in the right cerebral hemisphere with 50 μl of 5×10^3 tissue culture infectious units of BDV strain He/80-1 (NBD) or phosphate-buffered saline (PBS) (sham-inoculated rats [control]). Rats were sacrificed at PND21, PND28, PND42, and PND84 for nucleic acid, protein, and anatomic analyses.

RNA extraction. At PND28 postinoculation, NBD ($n = 7$) and control ($n = 5$) rats were terminally anesthetized with CO_2. Brain regions (CBLM and HC) were immediately dissected, snap frozen in TRIzol (Invitrogen, Carlsbad, CA), and stored at −80°C. Following extraction using standard protocols, RNAs were quantitated by UV spectrophotometry.

Quantitative real-time PCR. Intron-exon-spanning, gene-specific PCR primers and fluorophore-labeled oligonucleotide probes specific for rat AldoC, phosphofructokinase C (PFK-C), EAAT4, and porphobilinogen deaminase (PBGD) as a housekeeping gene control were designed for real-time PCR, using Primer Express 1.0 software (Applied Biosystems, Foster City, CA) (Table 1). Probes were labeled with a 5′-end fluorescent reporter dye (6-carboxyfluorescein) and a 3′-end quencher dye (6-carboxytetramethylrhodamine). For determination of the target transcript copy number, PCR standards were created by subcloning the region of the gene to be analyzed into the pGEM-T Easy vector (Promega Corporation, Madison, WI). The linearized plasmid was quantitated by UV spectroscopy, and 10-fold serial dilutions were created in water containing yeast tRNA (1 ng/μl). The sensitivities of PCR standards ranged from 5×10^5 to 5×10^1 copies for AldoC, 5×10^5 to 5×10^0 copies for PFK-C, and 5×10^5 to 5×10^1 copies for EAAT4. RNAs from CBLM or HC of individual animals were used for real-time PCR assays. cDNAs were synthesized using Taqman reverse transcription reagents (Applied Biosystems) from cerebellar or hippocampal RNAs of individual NBD ($n = 7$) and control ($n = 5$) rats (2 μg RNA per 100-μl reaction mix), and each sample was assayed in triplicate. Each 25-μl amplification reaction mix contained 10 μl template cDNA, 12.5 μl universal master mix (Applied Biosystems), 200 nM probe, and the primer concentrations given in Table 1. The thermal cycling profile, using a model 7700 sequence detector system (Applied Biosystems), consisted of the following: stage 1, 1 cycle at 50°C for 2 min; stage 2, 1 cycle at 95°C for 10 min; and stage 3, 45 cycles at 95°C for 15 s and 60°C for 1 min. A PBGD transcript was amplified in triplicate reactions by real-time PCR on the same plate as the gene of interest. The mean concentration of PBGD in each sample was used to control for the integrity of input mRNAs and to normalize values of target gene expression to those for the housekeeping gene. Results were expressed as the mean numbers of copies per 200 ng total RNA for AldoC, PFK-C, and EAAT4 relative to the value obtained for PBGD mRNA. The specificity of each assay was confirmed by inclusion of a negative control lacking a cDNA template. PCRs were examined by 1.5% agarose gel electrophoresis for verification of single amplification products.

Western blot analysis. CBLM were dissected from PND28 NBD ($n = 4$) and control ($n = 4$) rats and homogenized in PBS or sodium dodecyl sulfate (SDS) buffer (for EAAT4 Western blots; 50 mM NaP_i, pH 7.4, 10 mg/ml SDS) containing protease inhibitors (Complete Mini EDTA-free tablets; Roche Molecular Biochemicals, Indianapolis, IN). Homogenates were centrifuged at 12,000 rpm for 15 min at 4°C. Supernatants were collected, and protein concentrations were estimated by the Bradford assay (Bio-Rad, Hercules, CA). Proteins from regional brain homogenates (20 μg) in sample buffer (10 mM Tris-HCl, pH 7.5, 10 mM EDTA, 20% [vol/vol] glycerol, 1% [wt/vol] SDS, 0.005% [wt/vol] bromphenol blue, 100 mM dithiothreitol) were boiled for 5 min and size fractionated by 10% SDS-polyacrylamide gel electrophoresis. Gels and nitrocellulose membranes were briefly equilibrated in transfer buffer (25 mM Tris-HCl, pH 8.3, 192 mM glycine, 15% methanol) before transfer of proteins to membranes using a semidry blotting apparatus (Owl Separation Systems, Portsmouth, NH). Membranes were blocked in 2% nonfat milk powder in TTBS (20 mM Tris-HCl, pH 7.6, 137 mM NaCl, 0.1% Tween 20) overnight at room temperature and incubated with rabbit anti-BDV nucleoprotein (N protein; 1:10,000) (11), rabbit

anti-BDV phosphoprotein (P protein; 1:10,000) (11), mouse monoclonal anti-zebrin II (1:50) (a kind gift of Richard Hawkes), or rabbit anti-rat EAAT4 (1:50) (Alpha Diagnostic International, San Antonio, TX) antibody (Ab) in TTBS containing 1% nonfat dry milk for 2 h at room temperature. Membranes were washed three times for 10 min each with TTBS prior to incubation with peroxidase-conjugated goat anti-mouse immunoglobulin G (IgG; 1:2,000) (Bio-Rad) or goat anti-rabbit IgG (Bio-Rad) (1:2,000) in TTBS with 1% nonfat dry milk for 1 h at room temperature. Membranes were washed again with TTBS, developed using an ECL Western blot detection system (Amersham Biosciences, Arlington Heights, IL), and scanned for chemiluminescence using a Storm 840 imager (Molecular Dynamics, Sunnyvale, CA). Blots were then stripped and reprobed with mouse anti-glyceraldehyde-3-phosphate dehydrogenase (anti-GAPDH) monoclonal antibody (Ambion, Austin, TX). Protein band signals were analyzed using Image Quant software (v. 1.0; Molecular Dynamics). The signals of individual protein bands were normalized to the GAPDH band intensity and represented in arbitrary units.

Histological analysis and immunofluorescence. Under CO_2 anesthesia, PND21, PND28, PND42, and PND84 NBD (n = 5/age group) and control (n = 4/age group) rats were perfused via left ventricular puncture with PBS (1 ml/g body weight), followed by buffered 4% paraformaldehyde (1 ml/g body weight). Tissues were removed, postfixed in 4% paraformaldehyde overnight at 4°C, and cryoprotected with graded sucrose solutions before being embedded in tissue freezing medium (Triangle Biomedical Sciences, Durham, NC). Cryostat sections (14 μm) were collected on glass slides (Super Frost Plus; Fisher Scientific, Pittsburgh, PA). Tissue sections were stained with hematoxylin and eosin (H&E) for histological analysis. For immunofluorescence, sections were rinsed for 5 min in PBS, followed by incubation with 0.1% Triton X-100 in PBS for 1 h at room temperature. Sections were again washed with PBS for 5 min, followed by blocking with 10% goat serum in PBS for 1 h at 37°C. Sections were incubated overnight at 4°C with the following primary antibodies in blocking solution: rabbit anti-BDV N protein (1:1,500), mouse monoclonal anti-zebrin II (1:50), rabbit anti-rat EAAT4 Ab (1:50) (Alpha Diagnostic International), rabbit anti-calbindin D-28K (1:100) (Chemicon, Temecula, CA), rabbit anti-GFAP Ab (1:100) (DAKO Cytomation, Carpinteria, CA), mouse anti-GFAP MAb cocktail (1:30) (BD Pharmingen, San Diego, CA), mouse OX-42 MAb (1:100) (Chemicon), rabbit anti-Iba1 Ab (1:100) (Wako Pure Chemical Industries, Ltd., Richmond, VA), mouse anti-horse MT-I/-II (1:50) (clone E9; DAKO Cytomation), and mouse anti-rat CD44H Ab (1:50) (BD Pharmingen). After three washes in PBS, sections were incubated with Cy3-conjugated anti-mouse IgG or Cy3-conjugated anti-rabbit IgG and/or Cy2-conjugated anti-rabbit IgG or Cy2-conjugated anti-mouse IgG (1:200) (Jackson Immunoresearch Laboratories, Inc., West Grove, PA) in PBS for 1 h at room temperature. Sections were washed three times in PBS, dehydrated through graded ethanol solutions, placed in Americlear (Richard-Allan Scientific, Kalamazoo, MI), and mounted with Permount (Fisher Scientific) for microscopic analysis. Images were obtained using a Nikon Eclipse E600 fluorescence microscope. Images were matched for brightness and contrast but were otherwise unaltered.

TUNEL. Cellular DNA fragmentation was labeled in brain sections by terminal deoxynucleotidyltransferase-mediated dUTP-biotin nick end labeling (TUNEL), using diaminobenzidine as the chromogen (23). Cryostat sections were fixed in 4% paraformaldehyde and treated with 1 μg/ml proteinase K (Roche, Indianapolis, IN) for 5 min at 37°C. Sections were washed with PBS, fixed in paraformaldehyde, treated with 0.3% hydrogen peroxide in 0.1 M phosphate buffer for 20 min, and dehydrated through graded ethanol solutions. Sections were covered with a mixture of 1 mM biotinylated-16-dUTP (Roche), 10 mM dATP (Roche), terminal deoxynucleotidyltransferase enzyme (Promega, Madison, WI), 5× terminal deoxynucleotidyltransferase buffer (Promega), and distilled H_2O and incubated at 37°C for 1 h. After washes with PBS, visualization of the reaction was carried out using a Vectastain Elite ABC kit (Vector Laboratories, Burlingame, CA), with diaminobenzidine as the substrate (Vector Laboratories), according to the manufacturer's instructions. Slides were counterstained with hematoxylin, mounted, and visualized with a light microscope at a magnification of ×100. Cells with intense brown nuclear staining or brown staining of fragmented DNA within the cell were scored as TUNEL positive.

Statistical analysis. Data are presented as means ± standard errors of the means. The significance of observed differences between NBD and control groups was assessed by analysis of variance (ANOVA) for real-time PCR and densitometric Western immunoblot analyses. Analysis was carried out using StatView software (v. 5.0.1; SAS Institute Inc., Cary, NC). Values were considered to be significant when the P values were <0.05.

RESULTS

Distribution of BDV antigen in NBD CBLM. Rats were infected with BDV in the first 12 h of life and sacrificed at the following time points for anatomic, RNA, and protein analyses: PND21 (3 weeks), PND28 (4 weeks), PND42 (6 weeks), and PND84 (12 weeks). Consistent with previous reports, neonatally infected rats had disturbances in growth and behavior, including asymmetric protoambulatory responses, delayed righting responses, increased locomotion, and increased stereotypies (7, 29). As noted in previous reports, the NBD CBLM was reduced in size (8, 17, 73). We assessed the distribution of BDV N protein in the CBLM of PND28 NBD (Fig. 1A and C) and control (Fig. 1B) rats by immunofluorescence histochemistry. At PND28, viral antigen was expressed in nearly all PCs (Fig. 1C, arrows) but was also detectable in numerous cells in the molecular layer (Fig. 1C, bracketed cells) and occasional cells in the granular layer (Fig. 1C, boxed cells).

Decreased cerebellar AldoC, PFK-C, and EAAT4 expression during NBD. Borna disease in infected immunocompetent adult Lewis rats is mediated by infiltrating T cells (12). In contrast, brain damage in neonatal infection occurs without overt immune cell infiltration (28). The CBLM is severely affected in NBD rats, with a loss of PCs and granule cell neurons. To investigate potential mechanisms of neural damage in neonatal infection, we assessed cerebellar mRNA expression profiles in NBD and control rats by using oligonucleotide microarrays. Preliminary microarray results indicated specific decreases for AldoC, EAAT4, and PFK-C mRNAs (data not shown). An age of 4 weeks was chosen for assessments, as it correlates temporally with early PC degeneration in CBLM (29).

Real-time PCR assays were established to evaluate levels of AldoC, EAAT4, and PFK-C mRNAs in individual PND28 NBD (n = 7) and control (n = 5) rat cerebella. Porphobilinogen deaminase mRNA served as a normalization control for transcript quantity and integrity. NBD rats had marked decreases in cerebellar AldoC mRNA (Fig. 1D) (1.98-fold; P = 0.0014 by ANOVA), EAAT4 mRNA (Fig. 1E) (2.74-fold; $P <$ 0.0001 by ANOVA), and PFK-C mRNA (Fig. 1F) (1.58-fold; P = 0.0044 by ANOVA). Western immunoblot analysis was employed to assess the protein levels of viral antigens, AldoC, and EAAT4 in extracts of NBD and control rat cerebella. The presence of BDV N and P proteins was confirmed by Western immunoblotting of NBD cerebellar homogenates (Fig. 1G). AldoC and EAAT4 proteins were decreased in NBD CBLM (Fig. 1G). Densitometric analysis of Western blots revealed a significant, 38% decrease in the AldoC signal (Fig. 1H) (P = 0.042 by ANOVA) and a 28% decrease in the EAAT4 signal (Fig. 1I) (P = 0.0063 by ANOVA) in NBD compared to control rats.

Distribution of PC loss in the AZ vermis. Our findings of decreased AldoC mRNA and protein in CBLM led us to investigate patterns of PC loss in relation to zebrin II expression domains. No differences were appreciated between NBD and control cerebella at PND21. Zebrin II-positive bands were apparent in the AZ vermis, and calbindin D-28K immunoreactivity was homogeneous in the PC and molecular layers (data not shown). In control rats at PND28, PND42, and PND84, immunofluorescence revealed the classical adult zebrin II

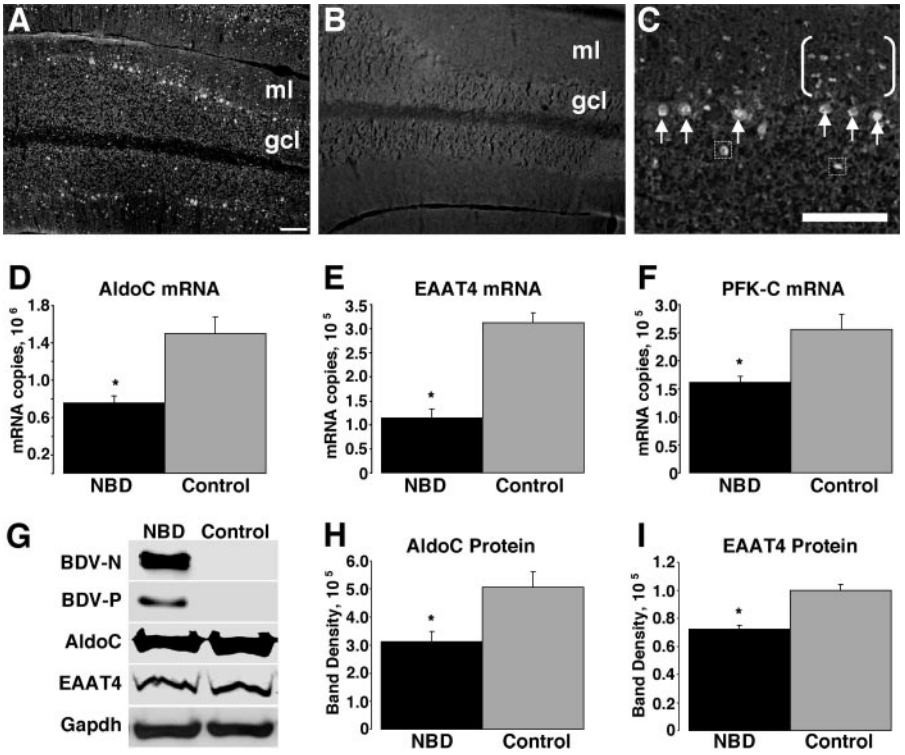

FIG. 1. Decreased AldoC, EAAT4, and PFK-C expression in the CBLM of NBD rats. Immunofluorescence analysis of the BDV N protein in CBLM of PND28 NBD (A and C) and control (B) rats is shown. Note the prominent staining of PCs (arrows in panel C) and unidentified cells in the molecular layer (bracketed cells in panel C) and granule cell layer (boxed cells in panel C). (D to F) Real-time PCR for AldoC, EAAT4, and PFK-C mRNAs, respectively, from PND28 NBD ($n = 7$) and control ($n = 5$) rat CBLM. (D) AldoC mRNA levels in PND28 CBLM, showing 1.98-fold decrease in NBD rats ($P = 0.0014$ by ANOVA). (E) EAAT4 transcript levels from PND28 cerebellar RNA, showing 2.74-fold decrease in NBD rats ($P < 0.0001$ by ANOVA). (F) PFK-C transcript levels from PND28 CBLM, showing 1.58-fold decrease in NBD rats ($P = 0.0044$ by ANOVA). (G) Western immunoblots for BDV N protein, BDV P protein, AldoC, EAAT4, and GAPDH (loading control). (H and I) Signal intensities from Western blots for AldoC and EAAT4, respectively, from PND28 cerebellar protein extracts from NBD ($n = 4$) and control ($n = 4$) rats. (H) AldoC protein levels are significantly decreased in PND28 NBD rat CBLM, with a 38% decrease in NBD compared to control rats ($P = 0.042$ by ANOVA). (I) EAAT4 protein levels are significantly decreased in PND28 NBD rat CBLM, with a 28% decrease in NBD compared to control rats ($P = 0.0063$ by ANOVA). Abbreviations: ml, cerebellar molecular layer; gcl, cerebellar granule cell layer. Asterisks, $P < 0.05$. Bars = 100 μm.

banding pattern (Fig. 2A and C) as well as homogeneous staining for calbindin in the PC and molecular layers (Fig. 2B and C). At PND28, zebrin II bands (P1 to P3) were largely conserved in NBD rat lobules I to V (Fig. 2D); however, gaps in the PC and molecular layers, indicative of PC loss, were revealed with calbindin staining (Fig. 2E). The findings with calbindin were consistent with previous reports documenting the inception of PC loss between PND27 and PND33 (80). Colocalization of zebrin II and calbindin in PND28 NBD rats revealed that PC loss was largely confined to the zebrin II-negative molecular phenotype (Fig. 2F and G; double-headed arrows in panel G define regions of PC loss). In the most affected lobules (e.g., lobules III and IV [Fig. 2G]), only rare PCs survived in zebrin II-negative zones and were often localized centrally between two zebrin II-positive bands (Fig. 2G, bracketed cells). At PND42, zebrin II-positive bands were no longer preserved in the NBD rat AZ vermis, with only a few surviving zebrin II-positive PCs observed (Fig. 2H, arrow). Calbindin staining in PND42 NBD rats revealed extensive PC loss compared to that at PND28 (Fig. 2I and J [merged image]). At PND84, the AZ vermis was devoid of zebrin II bands (Fig. 2K), and calbindin staining revealed only scattered surviving PCs (Fig. 2L and M [merged image]).

Distribution of PC loss in lateral cerebellar lobules. The preferential early survival of zebrin II-positive PCs in the vermes of NBD rats was not observed in lateral cerebellar regions (i.e., hemispheres, flocculi, and paraflocculi). Zebrin II and calbindin labeling was normal in control rat hemispheres (Fig. 3A to C). In NBD rats at PND28, PC losses in the hemispheres (simple lobule and crus I of the anciform lobule) were observed in both zebrin II-positive and -negative regions (Fig. 3D, arrows show the loss of zebrin II-positive PCs). Calbindin staining revealed small stripes of cell loss interdigitating with small stripes of cell survival (Fig. 3E, with cell loss indicated by arrows, and F [merged image]). Although PCs in the flocculus and paraflocculus were all zebrin II positive in control rats (Fig. 3G), these regions were severely affected in PND28 NBD rats. Numerous zebrin II-positive neurons were lost from these regions, resulting in large unstained gaps interdigitating with bands of surviving PCs (Fig. 3H).

Preferential PC survival in the nodular zone. Preferential conservation of lobule X PCs was previously reported for mu-

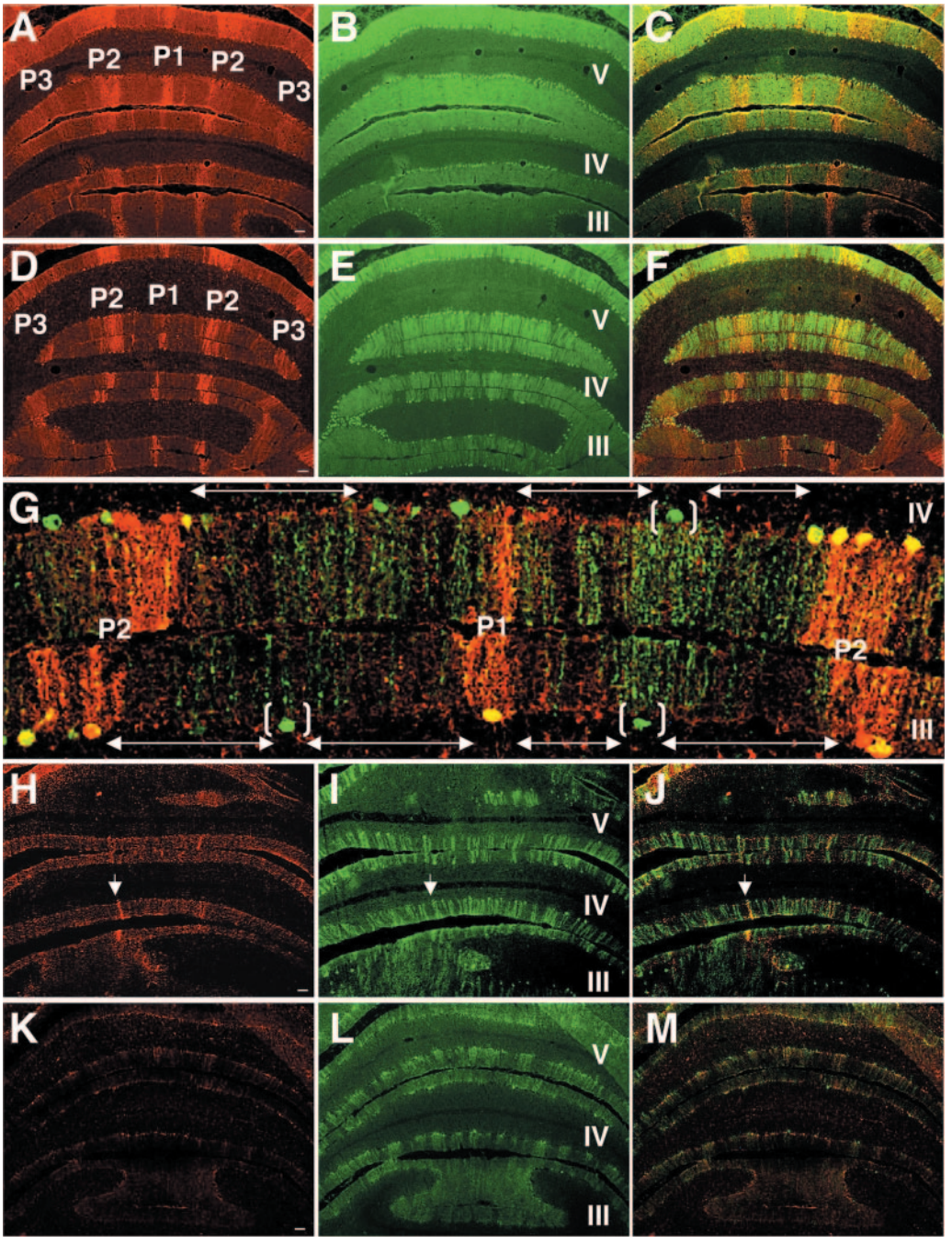

FIG. 2. Zebrin II-negative PC populations are lost preferentially in the AZ of PND28 NBD rats. Transverse sections through the anterior CBLM of PND28 control (A, B, C), PND28 NBD (D, E, F, G), PND42 NBD (H, I, J), and PND84 NBD (K, L, M) rats double labeled for zebrin II (A, D, H, K) and calbindin D28K (B, E, I, L), with merged signals (C, F, G, J, M), are shown. Zebrin II bands were consistently observed in control rats (A), and calbindin staining (B) was homogeneous in the molecular and PC layers (panels A and B merged in panel C). Zebrin II expression modules are largely preserved in PND28 NBD rats (D) (note the P1 to P3 bands in lobules III to V), despite numerous small and large gaps in the PC layer detected with calbindin staining (E). (F) Colocalization of signals revealed the specific loss of PCs in zebrin II-negative zones. (G) High-magnification view of lobules III and IV (P1 and P2 bands) from a PND28 NBD rat, double labeled for zebrin (red) and calbindin (green). Note the large gaps in the PC layer indicated by double-headed arrows and the few surviving zebrin II-negative PCs, localized approximately equidistant between zebrin II-positive bands (bracketed cells). (H) Zebrin II staining in PND42 NBD rats reveals a nearly complete loss of zebrin expression domains (the arrow indicates a surviving zebrin II-positive neuron in lobule IV from the P2 band). (I) Calbindin staining in PND42 NBD rat reveals extensive loss of PCs, resulting in large gaps in the PC and molecular layers (panels H and I merged in panel J). (K) Zebrin II staining in PND84 NBD rat shows a complete loss of zebrin II domains and decreased background. (L) Few surviving PCs were evident with calbindin staining in the AZ of PND84 NBD rats (panels K and L merged in panel M). Bars = 100 μm.

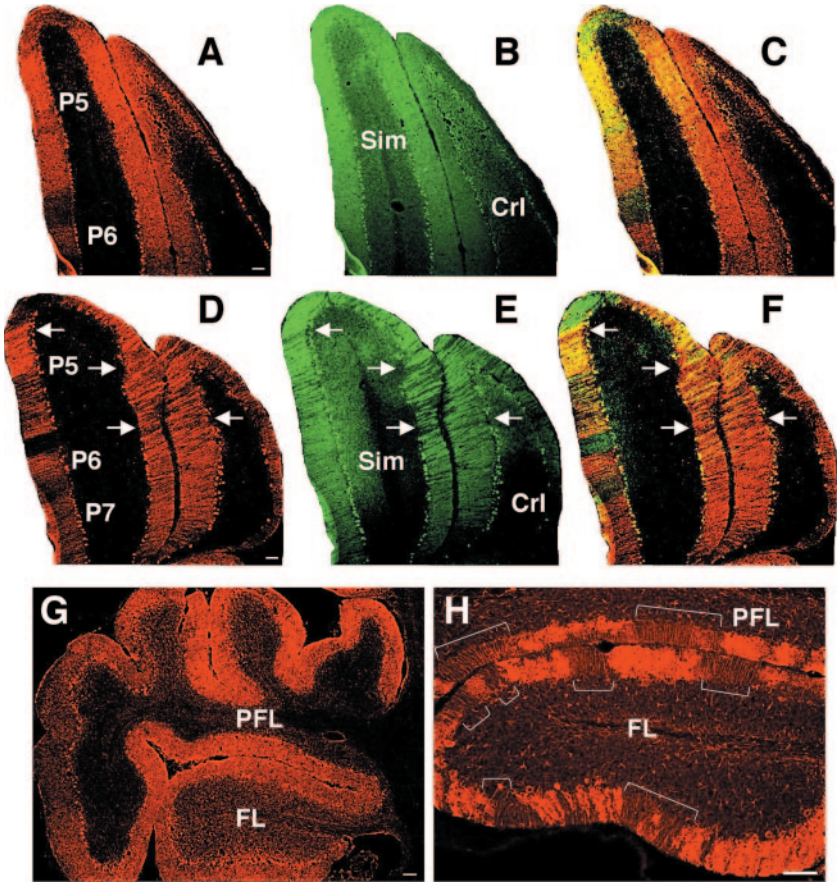

FIG. 3. Loss of zebrin II subsets in hemispheres, flocculi, and paraflocculi. Double-label immunofluorescence for zebrin II (A, D) and calbindin (B, E) in PND28 control (A, B, C) and PND28 NBD (D, E, F) rats, with merged images (C, F), is shown. Note the loss of zebrin II-positive neurons in the simple lobule and crus I of the anciform lobule in NBD rats (arrows in panels D, E, and F). (G) All PCs in the flocculus and paraflocculus were positive for zebrin II and EAAT4 in a control rat brain. Representative zebrin II staining is shown. (H) Cell loss in PND28 NBD rat flocculus and paraflocculus. Note the large gaps in PC and molecular layers (brackets) observed with zebrin II and EAAT4 staining. Representative zebrin II staining is shown. Abbreviations: Sim, simple lobule; CrI, crus I of the anciform lobule; PFL, paraflocculus; FL, flocculus. Bars = 100 μm.

tant models (i.e., nervous, pcd, shaker, toppler, and NPC1) and other diseases (i.e., X-chromosome-linked copper malabsorption, multiple systems atrophy, and spinocerebellar ataxia 6) (14, 16, 31, 34, 59, 68, 72, 75, 79). Therefore, we assessed PC loss in the NZ of NBD rats in relation to zebrin II expression modules.

Zebrin II expression and PC density (assessed by calbindin staining) were normal in control rat PZ and NZ at PND21, PND28, PND42, and PND84 (Fig. 4A, B, and C). In control rats, characteristic thick bands of zebrin II-positive PCs and thin bands of zebrin II-negative PCs were observed in lobules VIII and IX. All PCs were zebrin II positive in lobule X (Fig. 4A). Although modest PC losses in the PZ and NZ were apparent in NBD rats as early as PND28, differences between NBD and control rats were readily appreciated at PND42 (data not shown). At PND84, numerous surviving zebrin II-positive PCs were observed in lobule X (Fig. 4D, E, and F). While PCs in lobule X were not entirely spared, survival was more substantial than that in the AZ, PZ, and lateral CBLM.

Loss of EAAT4 PC phenotypes. EAAT4 mRNA and protein levels were decreased in PND28 NBD rat CBLM (see above). Thus, we investigated patterns of EAAT4 expression in relation to zebrin II expression in the CBLM. EAAT4 immunostaining (Fig. 5A) in control rats corresponded with zebrin II-positive neurons (Fig. 5B and C), as previously reported (40). At PND28, EAAT4-positive bands were preserved in NBD rats (Fig. 5D) and colocalized with zebrin II bands (Fig. 5E and F). Surprisingly, a marked loss of EAAT4 staining was visible in zones corresponding to zebrin II-negative PCs in the AZ vermis (Fig. 5F, arrows define regions where EAAT4 staining is lost in zebrin II-negative zones). EAAT4 is likely expressed in zebrin II-negative PCs, but at lower levels than those of zebrin II-positive PCs. Background staining for EAAT4 was consistently higher in NBD rats. Increased background staining may reflect the modulation of low levels of specific glial or PC staining for EAAT4 in zebrin II-negative regions. The loss of EAAT4-negative and -positive PCs in lateral cerebellar regions at PND28 followed a similar pattern of PC loss to that found for zebrin II and calbindin (data not shown). By PND84, EAAT4 banding was completely abolished in the AZ vermis (Fig. 5G). The loss of EAAT4-positive stripes coincided with the loss of zebrin II-positive stripes (Fig. 5H and I).

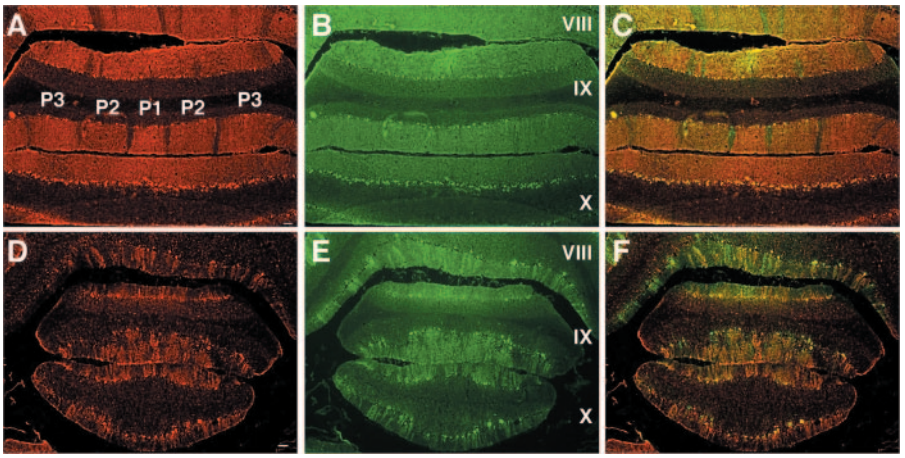

FIG. 4. PC survival in the NZ of NBD rats. Double-label immunofluorescence for zebrin II (A, D) and calbindin (B, E) in PND84 control (A, B, C) and PND84 NBD (D, E, F) rat lobules VIII, IX, and X, with merged images (C, F), is shown. Bars = 100 μm.

Astrocytic EAAT4 expression. EAAT4 expression in normal rats is reported to be confined predominantly to PCs; however, its expression has also been reported for astrocytes in the retina, spinal cord, forebrain, hindbrain, and primary cultures (30). EAAT4 staining in NBD rat CBLM revealed numerous EAAT4-immunoreactive cells with glial morphology. Thus, EAAT4 expression in glia was examined by double-label immunofluorescence, using antibodies directed against OX-42 and GFAP to distinguish microglia and astrocytes, respectively. No EAAT4-positive microglia were identified in either control or NBD rats. In NBD rats, EAAT4 was detected in Bergmann glial fibers in the molecular layer (Fig. 5J, K, and L, arrows) and in numerous reactive astrocytes in the granule cell layer (Fig. 5J, K, and L, boxed cell). No EAAT4 labeling was detected in cerebellar astrocytes or Bergmann fibers in control rats.

Astrogliosis is prominent throughout the brains of NBD rats; thus, we investigated EAAT4 levels outside the CBLM. Real-time PCR analysis of EAAT4 mRNA levels in HC revealed a significant increase in PND28 NBD rats compared to that in controls (Fig. 5M) (2.3-fold; $P = 0.0329$ by ANOVA). Hippocampal EAAT4 fluorescence was prominently increased in astrocytes in the dentate gyrus, hilus, and stratum lacunosum moleculare (Fig. 5N). Astrocytic EAAT4 expression was also observed, though to a lesser extent, in the cortex, caudate putamen, corpus collosum, and thalamic regions in NBD rats (data not shown). In control rats, faint EAAT4 staining was confined to scattered hilar astrocytes in the HC (Fig. 5O).

Compartmental expression of MT-I/II and CD44 by Bergmann glia and microglial activation. We have previously shown that metallothionein-I/II (MT-I/II) mRNA and protein are dramatically increased in NBD rat brains. The largest increase in MT-I/II mRNA was found in the CBLM, where MT-I/II protein localized to reactive astrocytes and Bergmann glia (78). Thus, we investigated the expression of MT-I/II in the CBLM to determine whether patterns of Bergmann glial MT-I/II expression correlated with compartmentalization in the CBLM. Immunofluorescence analysis revealed that MT-I/II expression in NBD Bergmann glia was compartmentalized in the vermis, forming bands of MT-I/II expression in the Bergmann glial cell bodies and fibers (Fig. 6A). We next examined the expression of MT-I/II with respect to EAAT4 (Fig. 6B, C, and D). MT-I/II was highly expressed in regions corresponding to EAAT4-negative zones, where the majority of PC loss occurred. Only small areas of overlap were observed between EAAT4 and MT-I/II (Fig. 6D, asterisk).

Previously, we have shown that the hyaluronan receptor CD44 was increased in the HC of NBD rats (78). However, the distribution of CD44 in the NBD rat CBLM has not been reported. Thus, we evaluated CD44 protein expression in the CBLM by immunofluorescence. CD44 staining was increased in NBD CBLM relative to that in controls (data not shown). Similar to MT-I/II staining, CD44 staining was increased in NBD Bergman glia and formed a banded pattern of expression (Fig. 6E) that was not observed in control rats (data not shown). In relation to EAAT4-positive bands (Fig. 6F), CD44 bands were largely confined to EAAT4-negative zones (Fig. 6G). However, CD44 bands often did not span the entire width of EAAT4-negative zones (Fig. 6G, asterisks). These results suggest that during disease states, Bergman glia may enhance programs of gene expression related to injury, forming distinct banding patterns similar to those found in PC subsets.

Microgliosis is a prominent feature in the brains of NBD rats. Thus, we investigated the distribution of microglia (anti-Iba1 immunofluorescence) in the NBD CBLM. In PND28 NBD rat CBLM, microglia aligned in a striped formation spanning the molecular layer (Fig. 6H, arrows). Bands of microglia were most prominent in the AZ vermis, consistent with selective, early PC loss in this region. Only faint staining of a few scattered microglia was observed in control rat cerebella (Fig. 6I). Stripes of microglia often aligned with infected PCs and were often found enwrapping PC somata (data not shown). The distribution of microglia (Fig. 6J, green) in relation to that of zebrin II (Fig. 6J, red) was examined by double-label immunofluorescence, using antibodies directed against microglia (Iba1) and zebrin II. This analysis revealed that microglial density and striping were greater in zebrin II-negative zones in the anterior vermes of PND28 NBD CBLM.

Spatial and morphological changes in PCs. Calbindin staining revealed abnormalities in PC distribution and morphology.

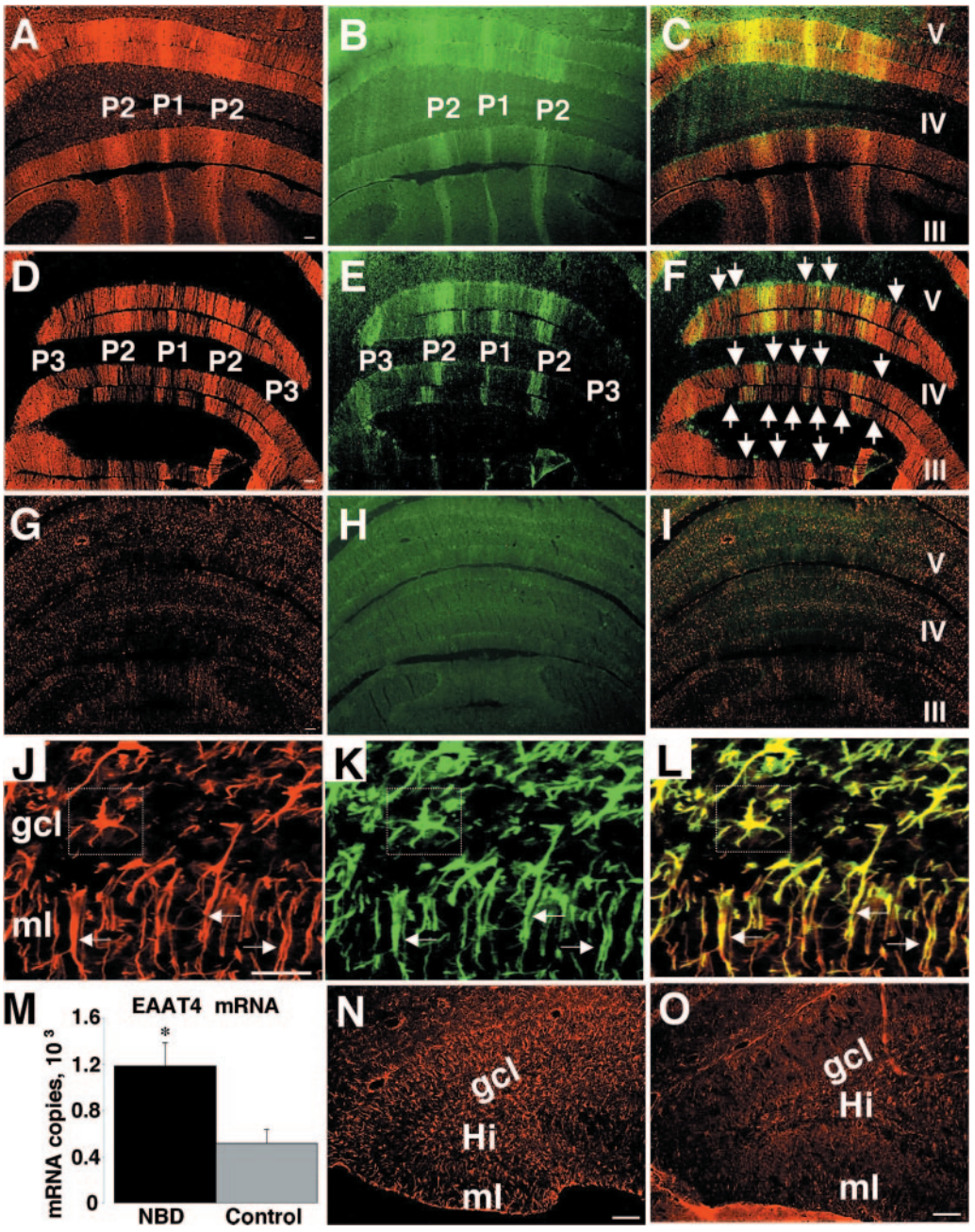

FIG. 5. Preservation of EAAT4-positive neurons in PND28 NBD rat vermis and astrocytic EAAT4 expression. Double-label immunofluorescence for EAAT4 (A, D, G) and zebrin II (B, E, H) in control (A, B, C), PND28 NBD (D, E, F), and PND84 NBD (G, H, I) rats, with merged images (C, F, I), is shown. Note the loss of EAAT4 staining in zones corresponding to zebrin II-negative PCs (arrows in panel F). Double-label fluorescence for EAAT4 (J [red]) and GFAP (K [green]) reveals colocalization (L) with Bergmann glial fibers in the molecular layer (arrows) and with astrocytes in the granule cell layer (boxed cell) of the CBLM. (M) Real-time PCR analysis of EAAT4 mRNA expression in HC of PND28 NBD ($n = 7$) and control ($n = 5$) rats, showing a 2.3-fold increase in NBD rats ($P = 0.0329$ by ANOVA). EAAT4 immunofluorescence in the dentate gyri of PND28 NBD (N) and control (O) rats is shown. Abbreviations: ml, molecular layer; gcl, granule cell layer; Hi, hilus fasciae dentate. Asterisk, $P < 0.05$. Bars = 100 μm.

PC ectopia, although infrequent, was only observed in NBD rats (Fig. 7A). In some PCs, primary dendrites were grossly swollen (Fig. 7B). At PND28 and thereafter, the dendritic arbor was stunted and did not span the width of the molecular layer (Fig. 7C, bars). In some PCs, calbindin staining was absent in somata but intact in dendrites (Fig. 7C, arrow). Swollen, vacuolated PC somata were common at PND84, with the highest frequencies in the posterior and nodular zones (Fig. 7D and E; PND84 control rat PCs are shown in Fig. 7F for comparison). At PND84, the spatial orientation of some PCs was aberrant, and cell bodies were displaced into the granule cell layer (Fig. 7G, bar).

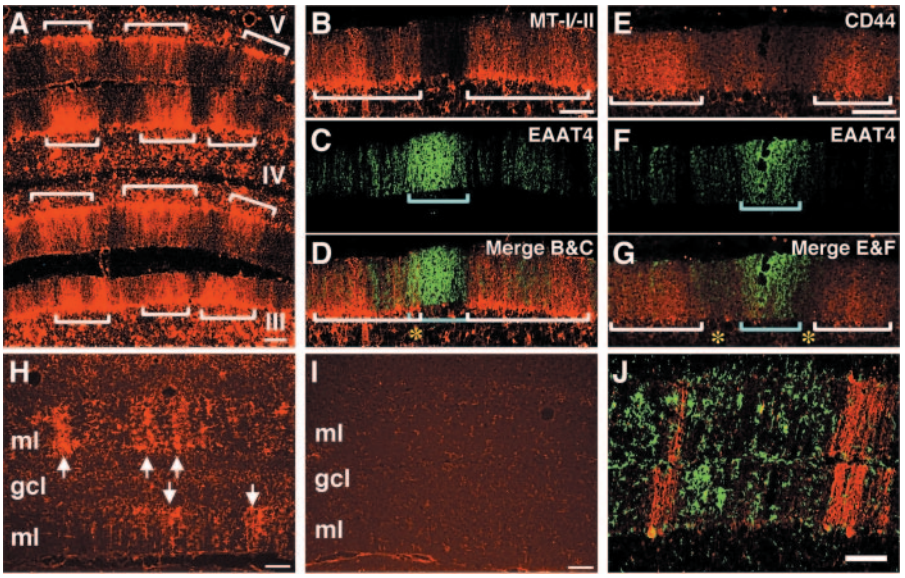

FIG. 6. Bergmann glial expression of MT-I/II and CD44 and density of microglia in zebrin II-negative zones. (A) MT-I/II fluorescence in the anterior vermis (lobules III to V) of PND28 NBD CBLM (note the banded distribution of MT-I/II in Bergmann glia [defined by brackets]). Double-label immunofluorescence for MT-I/II (B; white brackets define zones of high MT-I/II expression) and EAAT4 (C; blue bracket defines the EAAT4-positive zone) is shown. (D) Merged image showing MT-I/II expression largely confined to EAAT4-negative zones (the asterisk denotes a small region of overlap). Double-label immunofluorescence for CD44 (E; white brackets define zones of high CD44 expression) and EAAT4 (F; blue bracket defines the EAAT4-positive zone) is also shown. The merged image (G) shows CD44 expression in EAAT4-negative zones (asterisks denote EAAT4-negative zones where CD44 is absent). OX42 fluorescence of microglia in cerebellar vermes of PND28 NBD (H; arrows denote the striped pattern of microglial alignment) and control (I) rats is shown. Double-label immunofluorescence for OX-42 (J [green]) and zebrin II (J [red]) shows the high density of microglia in zebrin II-negative zones. Abbreviations: ml, molecular layer; gcl, granule cell layer. Bars = 100 μm.

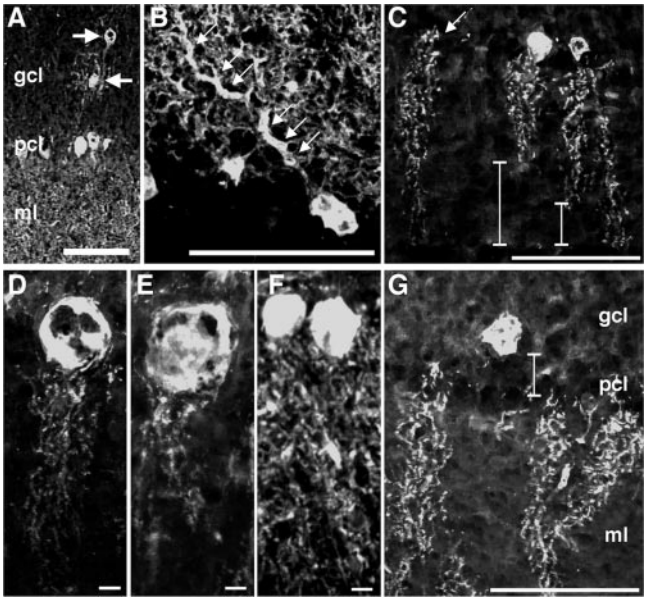

FIG. 7. PC spatial and morphological abnormalities in NBD rats. Calbindin D28K immunofluorescence in CBLM reveals ectopic PCs (A, arrows), swollen dendrites (B, arrows), retracted dendrites (C, bars), loss of PC somata (C, arrow), swollen PC somata in PND84 NBD rats (D and E) compared to those in PND84 control rat PCs (F), and PC somata retracted into the granule cell layer (G). Abbreviations: gcl, granule cell layer; pcl, Purkinje cell layer; ml, molecular layer. Bars = 100 μm (A, B, C, G) and 10 μm (D, E, F).

Apoptosis of PCs. Histological analysis of H&E-stained sections from PND28 NBD rats revealed prominent features of classical apoptosis in PCs, including nuclear pyknosis, cytoplasmic shrinkage, membrane blebbing (Fig. 8A and B), nuclear fragmentation (Fig. 8C), and formation of condensed chromatin balls (Fig. 8D). Similar morphological changes were observed in scattered cells of the molecular and granule cell layers (Fig. 8E). At PND84, PCs no longer showed classical signs of apoptosis and were often swollen with enlarged nuclei and cytoplasm (Fig. 8F). Morphological signs of apoptosis were not observed in control rat PCs (Fig. 8G). These findings were confirmed by TUNEL. TUNEL-positive PCs were observed in PND28 NBD rats (Fig. 8H, I, and J). Some TUNEL-positive PCs appeared to be at a stage when the nucleus had not fully disintegrated and were stained prominently by TUNEL (Fig. 8I). Other apoptotic PCs appeared to have lost intact nuclei, and diffuse, fragmented chromatin stained positively by TUNEL (Fig. 8J). Consistent with previous reports, granule cell neurons in the CBLM, dentate gyrus granule cell neurons, and cortical neurons also stained prominently by TUNEL at PND28 (29, 73; data not shown). No evidence of PC apoptosis was observed in control rats by TUNEL assay at PND21, PND28, or PND42 or in NBD rats at PND84.

DISCUSSION

PC loss is a prominent feature of several neurodevelopmental and neurodegenerative disorders, including autism, Alzheimer's disease, Huntington's disease, schizophrenia, epilepsy, and alcoholism (50, 58). The diversity of pathways contributing

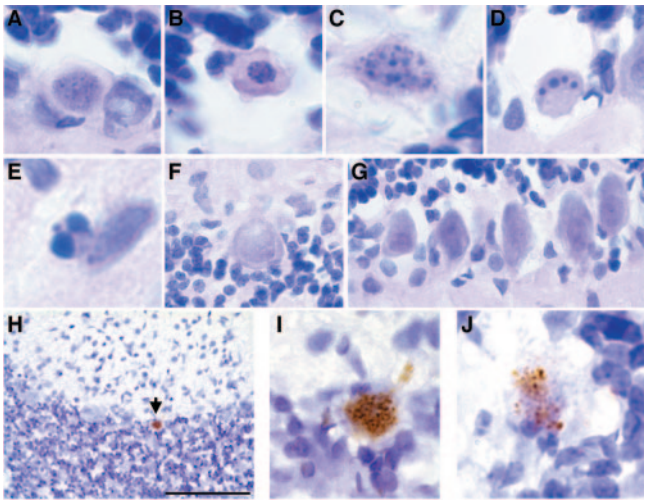

FIG. 8. PC apoptosis in NBD rats. Hematoxylin and eosin staining of cerebellar sections from PND28 NBD (A to E), PND84 NBD (F), and PND28 control (G) rats is shown. (A) H&E-stained PC with early signs of nuclear pyknosis. (B) H&E-stained PC with nuclear pyknosis, cytoplasmic shrinkage, and membrane blebbing. (C) H&E-stained PC with diffuse nuclear fragmentation. (D) H&E-stained PC with condensed chromatin balls. (E) H&E-stained cell in the molecular layer with nuclear fragmentation and chromatin condensation. (F) H&E-stained PC with swollen cytoplasm and nucleus from posterior cerebellar zone of PND84 NBD rat. (G) H&E-stained PCs from PND28 control rats. (H) TUNEL-positive PC (arrow) in anterior vermis of PND28 NBD rat. (I) High-magnification view of TUNEL-positive PC with compact labeling of fragmented DNA. (J) High-magnification view of TUNEL-positive PC with diffuse, fragmented DNA. Bar = 100 μm.

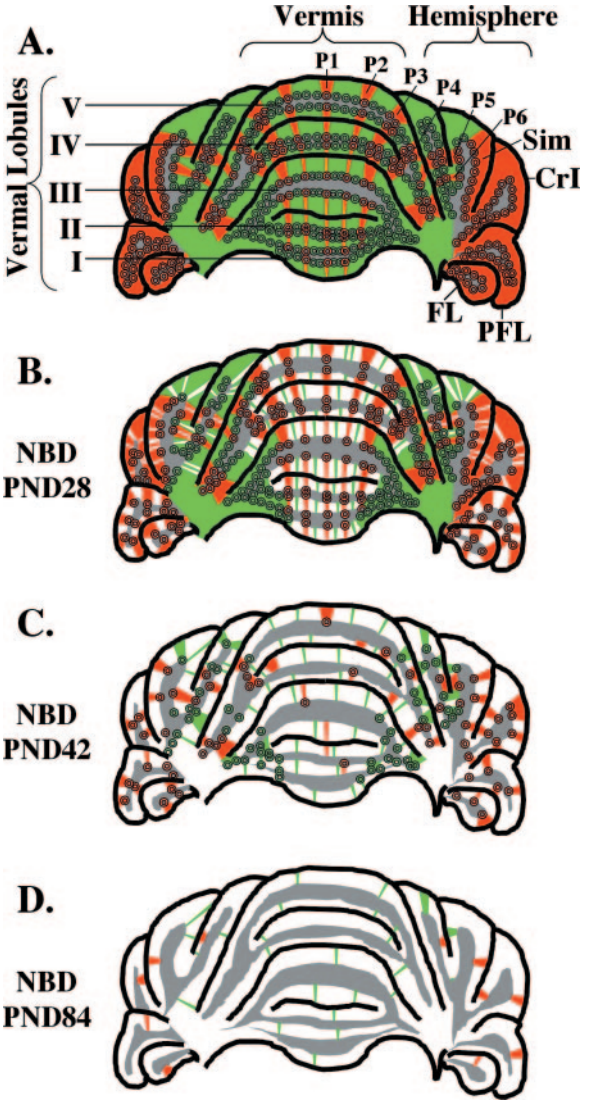

FIG. 9. Zonal PC loss in the anterior cerebellum over time in NBD rats. (A) Representation of the compartmental organization of zebrin-positive (red) and zebrin-negative (green) PC zones in the anterior cerebellum of control or PND21 NBD rats (preceding PC loss). The distribution of zebrin-positive zones P1 to P4 is shown for vermal lobules I to V, and zebrin-positive zones P5 and P6 are shown in the simple lobule (Sim). Note that all PCs in the flocculus (FL), paraflocculus (PFL), and crus I of the anciform lobule (CrI) are zebrin positive. (B) Distribution of PC loss in PND28 NBD rats. In the vermis, numerous PCs are lost (white) from zebrin-negative zones (note few surviving PCs [green bands]), while zebrin-positive PCs are largely preserved. In the hemispheres, random losses of both zebrin-negative and zebrin-positive PCs are observed. In the flocculus and paraflocculus, zones of zebrin-positive PC loss interdigitate with zones of zebrin-positive PC survival. (C) Representative PC loss in PND42 NBD rats. As PC loss progresses, the banded distribution of zebrin-positive PCs is disrupted in the vermis, and the loss of both PC subsets continues in the hemispheres. (D) Representative PC loss in PND84 NBD rats. At PND84, zebrin-positive PCs are no longer detectable in the vermis, and few surviving PCs remain in the anterior cerebellum. In panels A to D, gray indicates the location of the granule cell layer. Losses of granule cells are not represented in this figure. Abbreviations: Sim, simple lobule; CrI, crus I of the anciform lobule; PFL, paraflocculus; FL, flocculus.

to PC damage is underscored by numerous animal models based on naturally occurring mutations (e.g., *Leaner*, *tottering*, *pogo*, *nervous*, *weaver*, and *tambaleante* mice), transgenic expression (e.g., *SCA1*, *MJD1*, and *SV40 large T antigen* mice), gene knockout (e.g., *Acid sphingomyelinase*, *XPG*, and *mottled*), intoxication (e.g., Ibogaine, OX7-saporin, phencyclidine, acrylamide, and methotrexate), ischemia, and viral infection (10, 17, 44, 58). In this study, we investigated patterns of PC death relative to parasagittal expression domains (Fig. 9A) following neonatal infection of rats with BDV. This investigation revealed preferential, early survival of zebrin II/EAAT4-positive PCs and preferential death of zebrin II/EAAT4-negative PCs in the vermes of NBD rats (Fig. 9B). Consistent with these findings, Bergmann glial expression of MT-I/II and CD44, as well as the density of microglia, was higher in zebrin II/EAAT4-negative zones. In contrast, early loss of PCs in the lateral CBLM and PC loss in the vermis at later stages of disease were not defined by antigenic compartments (Fig. 9B and C). Complete dissolution of zebrin II/EAAT4 banding was apparent in the AZ vermes of NBD rats by PND84 (Fig. 9D). As in other models of cerebellar degeneration, we observed relative sparing of PCs in lobule X. Extending these findings, we have characterized the glial expression of EAAT4, assessed spatial and morphological abnormalities of PCs, and demonstrated apoptotic degeneration of PCs in NBD rats.

Preferential early survival of zebrin II/EAAT4-positive PCs in the vermis. At PND28, PC loss in the cerebellar vermes of NBD rats was primarily confined to zebrin II/EAAT4-negative regions. Multifactorial processes are suggested to regulate pat-

terned death of PCs, including energy failure, glutamate toxicity, climbing fiber-mediated excitotoxicity, and exclusive expression of other host proteins in PC subsets (e.g., p75, the low-affinity nerve growth factor receptor) (15, 24, 42, 69, 70, 71, 74, 76). Viral transformation and viral infection can cause metabolic changes in infected cells, resulting in enhanced glucose uptake and glycolytic flux and in depletion of intracellular ATP (5, 6, 19, 26, 63, 67). Decreased ATP levels may reflect a consumptive necessity in infected cells for efficient viral replication (i.e., viral DNA/RNA and polypeptide synthesis). We recently demonstrated the induction of ER stress and the associated apoptotic molecule Chop in PND28 NBD PCs (77). Proper protein folding in the ER is dependent on ATP, and the ER is highly sensitive to stresses that perturb cellular energy levels (22, 27). Thus, PC subsets expressing large amounts of the glycolytic enzyme AldoC could have a selective advantage for responding to the increased energy demands associated with viral replication or ER stress. The decrease in mRNA encoding PFK-C, the rate-limiting enzyme in glycolysis, may support a role for energy failure in NBD neuropathology; however, the metabolic consequences of persistent BDV infection have not been determined. Alternatively, EAAT4 localizes to the same PCs that express AldoC, functions to reduce extracellular glutamate concentrations, and defines functionally and physiologically distinct compartments in the CBLM (40, 71, 74). Thus, EAAT4-positive PCs may possess a greater capacity for clearing excitotoxic glutamate from their synapses. This could contribute to the preferential survival of zebrin II/EAAT4-positive PCs in PND28 NBD rats as well as the long-term survival of PCs in lobule X, where all PCs are EAAT4 positive. As NBD progresses (i.e., PND42 and PND84), both zebrin II/EAAT4-negative and -positive PCs are rendered vulnerable to the virus-induced insult in the vermis, suggesting that the early survival advantage in zebrin II/EAAT4-positive zones is eventually overcome.

Patterns of PC loss in lateral cerebellar lobules. Neurodegeneration in NBD is largely confined to neurons that undergo substantial postnatal maturation, suggesting that maturational status may determine the susceptibility to damage. Cerebellar hypoplasia in NBD rats correlates with the dropout of PCs and their dendrites as well as the loss of the external and internal granule cell layers (8, 17). Our findings that early PC loss begins at around PND28 are in agreement with previous reports (80). However, granule cell loss is evident much earlier (PND14) (8). PCs are infected as early as PND3, possibly leading to functional impairment of PCs that could influence granule cell migration or maturation (8, 17, 73). Evidence suggests that PC integrity during an early critical period of development controls granule cell generation and survival (64). While BDV infection of PND1 rats results in dramatic cerebellar hypoplasia associated with the loss of PCs and granule cells, the cerebella of rats infected on PND15 are not hypoplastic (53). It is unclear whether preservation of the cerebella in this late-infection model is associated with enhanced survival of PCs, granule cells, or both. Nonetheless, these findings suggest that neuronal susceptibility to damage in infected rats is dependent on the maturational status of the cerebellum at the time of infection, with greater susceptibility during an early critical period. Additionally, for neonatal mice infected with BDV, BDV mRNAs are undetectable in the brains until after PND15, and overt cerebellar damage is not observed in neonatally infected mutant mice lacking functional $CD8^+$ T cells (25, 60). These findings suggest a slower spread of virus in mouse than in rat brains and support the importance of maturational status as a determinant of cerebellar neurodegeneration.

Preferential loss of zebrin II/EAAT4-negative PCs was not observed at PND28 in lateral regions of the NBD CBLM (i.e., hemispheres, flocculi, and paraflocculi). Maturation also varies regionally in the cerebellum, which may explain the regional differences observed between the vermal and lateral PC losses. There are regional differences in the sites and times of origin, cytogenic and migratory gradients, and settling times of PCs. PCs in the hemispheres are formed earlier but settle later than PCs of the vermis. There is a rostral-to-caudal cytogenic gradient in the hemispheres and a caudal-to-rostral gradient in the vermis (2). Furthermore, zebrin expression varies regionally and temporally in early postnatal development. In the rat, a few clusters of zebrin II-positive PCs begin to appear in the posterior lobes of the vermis at PND6. Thereafter, zebrin II expression spreads rostrally to the anterior vermis and lastly to the hemispheres. All PCs are zebrin II positive by PND12. Mature striping patterns emerge with the gradual loss of zebrin II from defined PC subsets; the adult pattern of interdigitating zebrin II-positive and -negative zones is apparent at around PND20 (35). PC infection during NBD has been documented as early as PND3 (8, 17, 73), preceding the earliest expression of zebrin II. Thus, many PCs may become infected or sustain damage prior to attaining their mature zebrin phenotype. In the flocculus and paraflocculus, where all PCs are of the zebrin II/EAAT4-positive phenotype, large numbers of PCs were lost at PND28. While this differs from the patterns in the vermis, the pattern of PC loss in the flocculus and paraflocculus did not appear to be entirely random, as zones of PC loss interdigitated with zones of surviving PCs. While all PCs in these regions are of the same zebrin II/EAAT4-positive phenotype, these regions are highly organized into microzones of flocculovestibular, cerebellar corticonuclear, and olivoflocculus projections (4, 56). Thus, it is tempting to speculate that even in these lateral regions, early PC loss may be defined by inherent zonal organization in the CBLM.

Glia-specific changes in NBD. Alterations of glial activation or function during neurodevelopment may influence homeostatic neuronal signaling and contribute to neuropathogenesis in NBD. Astrocytes are essential for normal neuronal activity (3, 45, 61). Persistent BDV infection of primary feline cortical astrocytes results in inhibition of glutamate uptake (9). The localization of EAAT4 in Bergmann glia and reactive astrocytes in the brains of NBD rats in this study may suggest that in pathological states, astrocytic EAAT4 expression plays some compensatory role to control extracellular glutamate levels (66). To our knowledge, this is the first report documenting a banded expression of proteins in Bergmann glia. Enhanced expression of MT-I/II and CD44 in discrete parasagittal zones of Bergmann glia may suggest a complex interplay between genetically determined PC subsets and the regional induction of glial gene expression during pathological states. Activated microglia secrete cytokines/chemokines and reactive oxygen species into the extracellular milieu that can critically mediate neurodevelopment and neuronal damage (32, 51). Activated

microglia exert pathological effects on neural progenitor cells (18, 39), and specific to the CBLM, microglia promote developmental PC apoptosis via the production of superoxide ions (38). We found a prominent striped alignment of microglia in the CBLM of PND28 NBD rats, with the highest density of microglia in zebrin II/EAAT4-negative zones. The phenomenon of microglial striping in CBLM was previously reported following phencyclidine injection and traumatic brain injury (21, 41).

Morphology of PCs. Dendritic abnormalities were detected in PCs of NBD rats beginning at PND28. Although both axonal (i.e., focal axonal swellings or torpedoes) and dendritic changes are commonly associated with PC damage, dendritic changes predominate in NBD rats (52). Dendritic changes are also more prevalent in *toppler* mutant PCs (14). The appearance of swollen primary dendrites and/or shortened dendritic arbors was previously associated with PC loss in other mutant (i.e., *pogo* and *NPC1* mice), knockout (i.e., *ASMKO* mice), and toxicant (i.e., neonatal toxicity of phenytoin) models (33, 43, 57, 59). Since shortened dendrites were not apparent at PND21 in NBD rats and since dendritic arbors reach adult dimensions in the rat after PND15, it is unlikely that dendritic maturation is defective. It is more likely that dendritic arbors retract following maturation to adult dimensions. These results suggest that common morphological changes manifest during PC death, despite a diversity of initiating insults. However, it remains unclear whether these changes reflect similar downstream mechanisms of PC degeneration.

Our observation of TUNEL-positive PCs and morphological signs of classical apoptosis in PND28 NBD rats confirms the apoptotic mechanisms of neurodegeneration. At PND84, TUNEL-positive PCs were no longer observed, suggesting that the timing for identification of apoptotic loss may occur within a narrow window.

Conclusions. The NBD model provides a new tool for investigating the basis of selective vulnerability of specific PC subsets to viral damage during neonatal development. Although nearly all PCs are infected in the early stages of NBD, regionally selective loss of the zebrin II/EAAT4-negative phenotype may suggest differences in neuronal sensitivity to viral insult. Investigating the extent to which these differences reflect intrinsic properties of PCs during postnatal development or their interactions with other neurons, astrocytes, or microglia may provide insights into cerebellar development and circuitry and could lead to strategies for improving the outcome of infectious and inflammatory insults to the central nervous system during early life.

ACKNOWLEDGMENTS

We are grateful to Richard Hawkes for his kind gift of anti-zebrin II antibodies and Cassandra M. Kirk for her expert technical assistance.

This work was supported by NIH awards NS29425 (W.I.L.), HD37546 (W.I.L.), and MH01608 (M.H.).

REFERENCES

1. **Ahn, A. H., S. Dziennis, R. Hawkes, and K. Herrup.** 1994. The cloning of zebrin II reveals its identity with aldolase C. Development **120:**2081–2090.
2. **Altman, J., and S. A. Bayer.** 1985. Embryonic development of the rat cerebellum. III. Regional differences in the time of origin, migration, and settling of Purkinje cells. J. Comp. Neurol. **231:**42–65.
3. **Anderson, C. M., and R. A. Swanson.** 2000. Astrocyte glutamate transport: review of properties, regulation, and physiological functions. Glia **32:**1–14.
4. **Balaban, C. D., R. J. Schuerger, and J. D. Porter.** 2000. Zonal organization of flocculo-vestibular connections in rats. Neuroscience **99:**669–682.
5. **Bardeletti, G.** 1977. Respiration and ATP level in BHK21/13S cells during the earliest stages of rubella virus replication. Intervirology **8:**100–109.
6. **Bardell, D., and M. Essex.** 1974. Glycolysis during early infection with feline and human cells with feline leukemia virus. Infect. Immun. **9:**824–827.
7. **Bautista, J. R., G. J. Schwartz, J. C. De La Torre, T. H. Moran, and K. M. Carbone.** 1994. Early and persistent abnormalities in rats with neonatally acquired Borna disease virus infection. Brain Res. Bull. **34:**31–40.
8. **Bautista, J. R., S. A. Rubin, T. H. Moran, G. J. Schwartz, and K. M. Carbone.** 1995. Developmental injury to the cerebellum following perinatal Borna disease virus infection. Brain Res. Dev. Brain Res. **90:**45–53.
9. **Billaud, J. N., C. Ly, T. R. Phillips, and J. C. de la Torre.** 2000. Borna disease virus persistence causes inhibition of glutamate uptake by feline primary cortical astrocytes. J. Virol. **74:**10438–10446.
10. **Bonthius, D. J., J. Mahoney, M. J. Buchmeier, B. Karacay, and D. Taggard.** 2002. Critical role for glial cells in the propagation and spread of lymphocytic choriomeningitis virus in the developing rat brain. J. Virol. **76:**6618–6635.
11. **Briese, T., C. G. Hatalski, S. Kliche, Y. S. Park, and W. I. Lipkin.** 1995. Enzyme-linked immunosorbent assay for detecting antibodies to Borna disease virus-specific proteins. J. Clin. Microbiol. **33:**348–351.
12. **Deschl, U., L. Stitz, S. Herzog, K. Frese, and R. Rott.** 1990. Determination of immune cells and expression of major histocompatibility complex class II antigen in encephalitic lesions of experimental Borna disease. Acta Neuropathol. (Berlin) **81:**41–50.
13. **Dittrich, W., L. Bode, M. Kao, and K. Schneider.** 1989. Learning deficiencies in Borna disease virus-infected but clinically healthy rats. Biol. Psych. **26:** 818–828.
14. **Duchala, C. S., H. E. Shick, J. Garcia, D. M. Deweese, X. Sun, V. J. Stewart, and W. B. Macklin.** 2004. The toppler mouse: a novel mutant exhibiting loss of Purkinje cells. J. Comp. Neurol. **476:**113–129.
15. **Dusart, I., M. P. Morel, and C. Sotelo.** 1994. Parasagittal compartmentation of adult rat Purkinje cells expressing the low-affinity nerve growth factor receptor: changes of pattern expression after a traumatic lesion. Neuroscience **63:**351–356.
16. **Edwards, M. A., J. E. Crandall, N. Leclerc, and M. Yamamoto.** 1994. Effects of nervous mutation on Purkinje cell compartments defined by zebrin II and 9-O-acetylated gangliosides expression. Neurosci. Res. **19:**167–174.
17. **Eisenman, L. M., R. Brothers, M. H. Tran, R. B. Kean, G. M. Dickson, B. Dietzschold, and D. C. Hooper.** 1999. Neonatal Borna disease virus infection in the rat causes a loss of Purkinje cells in the cerebellum. J. Neurovirol. **5:**181–189.
18. **Ekdahl, C. T., J. H. Claasen, S. Bonde, Z. Kokaia, and O. Lindvall.** 2003. Inflammation is detrimental for neurogenesis in adult brain. Proc. Natl. Acad. Sci. USA **100:**13632–13637.
19. **El-Bacha, T., M. M. Menezes, M. C. Azevedo e Silva, M. Sola-Penna, and A. T. Da Poian.** 2004. Mayaro virus infection alters glucose metabolism in cultured cells through activation of the enzyme 6-phosphofructo 1-kinase. Mol. Cell. Biochem. **266:**191–198.
20. **Ferguson, S. A.** 1996. Neuroanatomical and functional alterations resulting from early postnatal cerebellar insults in rodents. Pharmacol. Biochem. Behav. **55:**663–671.
21. **Fukuda, K., N. Aihara, S. M. Sagar, F. R. Sharp, L. H. Pitts, J. Honkaniemi, and L. J. Noble.** 1996. Purkinje cell vulnerability to mild traumatic brain injury. J. Neurotrauma **13:**255–266.
22. **Gaut, J. R., and L. M. Hendershot.** 1993. The modification and assembly of proteins in the endoplasmic reticulum. Curr. Opin. Cell Biol. **5:**589–595.
23. **Gavrieli, Y., Y. Sherman, and S. A. Ben-Sasson.** 1992. Identification of programmed cell death in situ via specific labeling of nuclear DNA fragmentation. J. Cell Biol. **119:**493–501.
24. **Gravel, C., L. M. Eisenman, R. Sasseville, and R. Hawkes.** 1987. Parasagittal organization of the rat cerebellar cortex: direct correlation between antigenic Purkinje cell bands revealed by mabQ113 and the organization of the olivocerebellar projection. J. Comp. Neurol. **265:**294–310.
25. **Hallensleben, W., M. Schwemmle, J. Hausmann, L. Stitz, B. Volk, A. Pagenstecher, and P. Staeheli.** 1998. Borna disease virus-induced neurological disorder in mice: infection of neonates results in immunopathology. J. Virol. **72:**4379–4386.
26. **Hatanaka, M., R. J. Huebner, and R. V. Gilden.** 1969. Alterations in the characteristics of sugar uptake by mouse cells transformed by murine sarcoma viruses. J. Natl. Cancer Inst. **43:**1091–1096.
27. **Hernandez-Fonseca, K., and L. Massieu.** 2005. Disruption of endoplasmic reticulum calcium stores is involved in neuronal death induced by glycolysis inhibition in cultured hippocampal neurons. J. Neurosci. Res. **82:**196–205.
28. **Hirano, N., M. Kao, and H. Ludwig.** 1983. Persistent, tolerant or subacute infection in Borna disease virus-infected rats. J. Gen. Virol. **64:**1521–1530.
29. **Hornig, M., H. Weissenbock, N. Horscroft, and W. I. Lipkin.** 1999. An infection-based model of neurodevelopmental damage. Proc. Natl. Acad. Sci. USA **96:**12102–12107.
30. **Hu, W. H., W. M. Walters, X. M. Xia, S. A. Karmally, and J. R. Bethea.** 2003. Neuronal glutamate transporter EAAT4 is expressed in astrocytes. Glia **44:**13–25.

31. **Iwata, M., A. Hirano, and J. H. French.** 1979. Degeneration of the cerebellar system in X-chromosome-linked copper malabsorption. Ann. Neurol. **5:**542–549.
32. **Jana, M., X. Liu, S. Koka, S. Ghosh, T. M. Petro, and K. Pahan.** 2001. Ligation of CD40 stimulates the induction of nitric-oxide synthase in microglial cells. J. Biol. Chem. **276:**44527–44533.
33. **Jeong, Y. G., B. H. Hyun, and R. Hawkes.** 2000. Abnormalities in cerebellar Purkinje cells in the novel ataxic mutant mouse, pogo. Brain Res. Dev. Brain Res. **125:**61–67.
34. **Kume, A., A. Takahashi, Y. Hashizume, and J. Asai.** 1991. A histometrical and comparative study on Purkinje cell loss and olivary nucleus cell loss in multiple system atrophy. J. Neurol. Sci. **101:**178–186.
35. **Leclerc, N., C. Gravel, and R. Hawkes.** 1988. Development of parasagittal zonation in the rat cerebellar cortex: MabQ113 antigenic bands are created postnatally by the suppression of antigen expression in a subset of Purkinje cells. J. Comp. Neurol. **273:**399–420.
36. **Levisohn, L., A. Cronin-Golomb, and J. D. Schmahmann.** 2000. Neuropsychological consequences of cerebellar tumour resection in children: cerebellar cognitive affective syndrome in a paediatric population. Brain **123:**1041–1050.
37. **Lohof, A. M., N. Delhaye-Bouchaud, and J. Mariani.** 1996. Synapse elimination in the central nervous system: functional significance and cellular mechanisms. Rev. Neurosci. **7:**85–101.
38. **Marin-Teva, J. L., I. Dusart, C. Colin, A. Gervais, N. van Rooijen, and M. Mallat.** 2004. Microglia promote the death of developing Purkinje cells. Neuron **41:**535–547.
39. **Monje, M. L., H. Toda, and T. D. Palmer.** 2003. Inflammatory blockade restores adult hippocampal neurogenesis. Science **302:**1760–1765.
40. **Nagao, S., S. Kwak, and I. Kanazawa.** 1997. EAAT4, a glutamate transporter with properties of a chloride channel, is predominantly localized in Purkinje cell dendrites, and forms parasagittal compartments in rat cerebellum. Neuroscience **78:**929–933.
41. **Nakki, R., J. Koistinaho, F. R. Sharp, and S. M. Sagar.** 1995. Cerebellar toxicity of phencyclidine. J. Neurosci. **15:**2097–2108.
42. **O'Hearn, E., and M. E. Molliver.** 1993. Degeneration of Purkinje cells in parasagittal zones of the cerebellar vermis after treatment with ibogaine or harmaline. Neuroscience **55:**303–310.
43. **Ohmori, H., H. Ogura, M. Yasuda, S. Nakamura, T. Hatta, K. Kawano, T. Michikawa, K. Yamashita, and K. Mikoshiba.** 1999. Developmental neurotoxicity of phenytoin on granule cells and Purkinje cells in mouse cerebellum. J. Neurochem. **72:**1497–1506.
44. **Oster-Granite, M. L., and R. M. Herndon.** 1985. The pathogenesis of parvovirus-induced cerebellar hypoplasia in the Syrian hamster, Mesocricetus auratus. Fluorescent antibody, foliation, cytoarchitectonic, Golgi and electron microscopic studies. J. Comp. Neurol. **169:**481–522.
45. **Parpura, V., T. A. Basarsky, F. Liu, K. Jeftinija, S. Jeftinija, and P. G. Haydon.** 1994. Glutamate-mediated astrocyte-neuron signalling. Nature **369:**744–747.
46. **Pletnikov, M. V., S. A. Rubin, K. Vasudevan, T. H. Moran, and K. M. Carbone.** 1999. Developmental brain injury associated with abnormal play behavior in neonatally Borna disease virus-infected Lewis rats: a model of autism. Behav. Brain Res. **100:**43–50.
47. **Pletnikov, M. V., S. A. Rubin, G. J. Schwartz, T. H. Moran, T. J. Sobotka, and K. M. Carbone.** 1999. Persistent neonatal Borna disease virus (BDV) infection of the brain causes chronic emotional abnormalities in adult rats. Physiol. Behav. **66:**823–831.
48. **Pletnikov, M. V., S. A. Rubin, K. M. Carbone, T. H. Moran, and G. J. Schwartz.** 2001. Neonatal Borna disease virus infection (BDV)-induced damage to the cerebellum is associated with sensorimotor deficits in developing Lewis rats. Brain Res. Dev. Brain Res. **126:**1–12.
49. **Raine, C. S., and B. N. Fields.** 1973. Reovirus type III encephalitis—a virologic and ultrastructural study. J. Neuropathol. Exp. Neurol. **32:**19–33.
50. **Reyes, M. G., and A. Gordon.** 1981. Cerebellar vermis in schizophrenia. Lancet **ii:**700–701.
51. **Rock, R. B., G. Gekker, S. Hu, W. S. Sheng, M. Cheeran, J. R. Lokensgard, and P. K. Peterson.** 2004. Role of microglia in central nervous system infections. Clin. Microbiol. Rev. **17:**942–964.
52. **Rossi, F., A. Jankovski, and C. Sotelo.** 1995. Target neuron controls the integrity of afferent axon phenotype: a study on the Purkinje cell-climbing fiber system in cerebellar mutant mice. J. Neurosci. **15:**2040–2056.
53. **Rubin, S. A., J. R. Bautista, T. H. Moran, G. J. Schwartz, and K. M. Carbone.** 1999. Viral teratogenesis: brain developmental damage associated with maturation state at time of infection. Brain Res. Dev. Brain Res. **112:**237–244.
54. **Rubin, S. A., P. Sylves, M. Vogel, M. Pletnikov, T. H. Moran, G. J. Schwartz, and K. M. Carbone.** 1999. Borna disease virus-induced hippocampal dentate gyrus damage is associated with spatial learning and memory deficits. Brain Res. Bull. **48:**23–30.
55. **Rubin, S. A., M. Pletnikov, R. Taffs, K. E. Wright, E. G. Brown, and K. M. Carbone.** 2000. Evaluation of a neonatal rat model for prediction of mumps virus neurovirulence in humans. J. Virol. **74:**5382–5384.
56. **Ruigrok, T. J., R. J. Osse, and J. Voogd.** 1992. Organization of inferior olivary projections to the flocculus and ventral paraflocculus of the rat cerebellum. J. Comp. Neurol. **316:**129–150.
57. **Sarna, J., S. R. Miranda, E. H. Schuchman, and R. Hawkes.** 2001. Patterned cerebellar Purkinje cell death in a transgenic mouse model of Niemann Pick type A/B disease. Eur. J. Neurosci. **13:**1873–1880.
58. **Sarna, J. R., and R. Hawkes.** 2003. Patterned Purkinje cell death in the cerebellum. Prog. Neurobiol. **70:**473–507.
59. **Sarna, J. R., M. Larouche, H. Marzban, R. V. Sillitoe, D. E. Rancourt, and R. Hawkes.** 2003. Patterned Purkinje cell degeneration in mouse models of Niemann-Pick type C disease. J. Comp. Neurol. **456:**279–291.
60. **Sauder, C., D. P. Wolfer, H. P. Lipp, P. Staeheli, and J. Hausmann.** 2001. Learning deficits in mice with persistent Borna disease virus infection of the CNS associated with elevated chemokine expression. Behav. Brain Res. **120:**189–201.
61. **Schell, M. J., M. E. Molliver, and S. H. Snyder.** 1995. D-Serine, an endogenous synaptic modulator: localization to astrocytes and glutamate-stimulated release. Proc. Natl. Acad. Sci. USA **92:**3948–3952.
62. **Schmahmann, J. D.** 1991. An emerging concept. The cerebellar contribution to higher function. Arch. Neurol. **48:**1178–1187.
63. **Singh, V. N., M. Singh, J. T. August, and B. L. Horecker.** 1974. Alterations in glucose metabolism in chick-embryo cells transformed by Rous sarcoma virus: intracellular levels of glycolytic intermediates. Proc. Natl. Acad. Sci. USA **71:**4129–4132.
64. **Smeyne, R. J., T. Chu, A. Lewin, F. Bian, S. Crisman, C. Kunsch, S. A. Lira, and J. Oberdick.** 1995. Local control of granule cell generation by cerebellar Purkinje cells. Mol. Cell. Neurosci. **6:**230–251.
65. **Takano, T., M. Uno, T. Yamano, and M. Shimada.** 1994. Pathogenesis of cerebellar deformity in experimental Chiari type I malformation caused by mumps virus. Acta Neuropathol. **87:**168–173.
66. **Takayasu, Y., M. Iino, W. Kakegawa, H. Maeno, K. Watase, K. Wada, D. Yanagihara, T. Miyazaki, O. Komine, M. Watanabe, K. Tanaka, and S. Ozawa.** 2005. Differential roles of glial and neuronal glutamate transporters in Purkinje cell synapses. J. Neurosci. **25:**8788–8793.
67. **Terekhina, N. A., I. Petrovich, and T. G. Parkhomenko.** 1998. Glycolytic metabolites and adenosine triphosphoric acid in the herpes-infected eye. Zh. Mikrobiol. Epidemiol. Immunobiol. **2:**92–94.
68. **Tolbert, D. L., M. W. Bradley, E. G. Tolod, I. Torres-Aleman, and B. R. Clark.** 2001. Chronic intraventricular infusion of glial cell line-derived neurotrophic factor (GDNF) rescues some cerebellar Purkinje cells from heredodegeneration. Exp. Neurol. **170:**375–379.
69. **Voogd, J., and T. J. Ruigrok.** 1997. Transverse and longitudinal patterns in the mammalian cerebellum. Prog. Brain Res. **114:**21–37.
70. **Voogd, J., J. Pardoe, T. J. Ruigrok, and R. Apps.** 2003. The distribution of climbing and mossy fiber collateral branches from the copula pyramidis and the paramedian lobule: congruence of climbing fiber cortical zones and the pattern of zebrin banding within the rat cerebellum. J. Neurosci. **23:**4645–4656.
71. **Wadiche, J. I., and C. E. Jahr.** 2005. Patterned expression of Purkinje cell glutamate transporters controls synaptic plasticity. Nat. Neurosci. **8:**1329–1334.
72. **Wassef, M., C. Sotelo, B. Cholley, A. Brehier, and M. Thomasset.** 1987. Cerebellar mutations affecting the postnatal survival of Purkinje cells in the mouse disclose a longitudinal pattern of differentially sensitive cells. Dev. Biol. **124:**379–389.
73. **Weissenbock, H., M. Hornig, W. F. Hickey, and W. I. Lipkin.** 2000. Microglial activation and neuronal apoptosis in bornavirus infected neonatal Lewis rats. Brain Pathol. **10:**260–272.
74. **Welsh, J. P., G. Yuen, D. G. Placantonakis, T. Q. Vu, F. Haiss, E. O'Hearn, M. E. Molliver, and S. A. Aicher.** 2002. Why do Purkinje cells die so easily after global brain ischemia? Aldolase C, EAAT4, and the cerebellar contribution to posthypoxic myoclonus. Adv. Neurol. **89:**331–359.
75. **Wenning, G. K., F. Tison, L. Elliott, N. P. Quinn, and S. E. Daniel.** 1996. Olivopontocerebellar pathology in multiple system atrophy. Mov. Disord. **11:**157–162.
76. **Wiesmann, C., and A. M. de Vos.** 2001. Nerve growth factor: structure and function. Cell. Mol. Life Sci. **58:**748–759.
77. **Williams, B. L., and W. I. Lipkin.** 2006. Endoplasmic reticulum stress and neurodegeneration in rats neonatally infected with Borna disease virus. J. Virol. **80:**8613–8626.
78. **Williams, B. L., K. Yaddanapudi, C. M. Kirk, A. Soman, M. Hornig, and W. I. Lipkin.** 2006. Metallothioneins and zinc dysregulation contribute to neurodevelopmental damage in a model of perinatal viral infection. Brain Pathol. **16:**1–14.
79. **Yang, Q., Y. Hashizume, M. Yoshida, Y. Wang, Y. Goto, N. Mitsuma, K. Ishikawa, and H. Mizusawa.** 2000. Morphological Purkinje cell changes in spinocerebellar ataxia type 6. Acta Neuropathol. (Berlin) **100:**371–376.
80. **Zocher, M., S. Czub, J. Schulte-Monting, J. C. de la Torre, and C. Sauder.** 2000. Alterations in neurotrophin and neurotrophin receptor gene expression patterns in the rat central nervous system following Borna disease virus infection. J. Neurovirol. **6:**462–477.